Generally polarized acoustic waves trapped by high aspect ratio electrode gratings at the surface of a piezoelectric material

V. Laude[a)]
Laboratoire de Physique et de Métrologie des Oscillateurs, CNRS UPR 3203, associé à l'Université de Franche-Comté, 32 avenue de l'Observatoire, 25044 Besançon cedex, France

A. Khelif
Laboratoire de Physique du Solide, Facultés Universitaires Notre-Dame de la Paix 61 rue de Bruxelles, 5000 Namur, Belgium

Th. Pastureaud and S. Ballandras
Laboratoire de Physique et de Métrologie des Oscillateurs, CNRS UPR 3203, associé à l'Université de Franche-Comté, 32 avenue de l'Observatoire, 25044 Besançon cedex, France

(Received 12 February 2001; accepted for publication 22 June 2001))

It has been shown theoretically and demonstrated experimentally that shear horizontal (SH) surface waves can exist when the surface of an isotropic substrate is perturbed by a strong corrugation, for instance consisting of deep grooves etched in the substrate, whereas these waves cannot exist without this perturbation. It is shown in this article that a periodic array of metallic electrodes (wires) exhibiting large aspect ratios deposited over a piezoelectric substrate give rise to surface acoustic waves with general polarization. The admittance of an interdigitated transducer, which is a basic tool for predicting the waves parameters, is calculated by a combination of finite element analysis and a boundary integral method. This approach has been extended to obtain the polarization of the acoustic waves. For different piezoelectric substrates, we predict various surface acoustic modes and their polarization. Along with mostly SH modes, we also find modes mostly polarized in the sagittal plane. We discuss the frequency behavior of the surface modes as a function of the electrode height compared to the period. © *2001 American Institute of Physics.*
[DOI: 10.1063/1.1394160]

I. INTRODUCTION

With the progress of techniques such as microlithography and electroplating, it is possible to create well defined micro- or nanostructures on an otherwise planar surface. These surface defects modify the physical properties of the crystal surface that in turn can serve as a tool for the characterization of the surface inhomogeneities. Several works have been devoted to the study of surface acoustic vibrations in presence of a single[1–4] or periodic[5–16] array of resonating elements. In particular, the periodically corrugated surface of an isotropic substrate can support localized shear horizontal (SH) modes, in contrast to the case of a substrate with a flat surface which can only guide Rayleigh waves of sagittal polarization. The propagation of surface acoustic waves (SAW) across a grating or a periodic array of wires deposited on a substrate is of great current interest for several reasons: the system is a model for a randomly rough surface that can be studied exactly and the results obtained in this work help to interpret the observations for a randomly rough surface. In the system such as investigated here, there can be a conversion of SAW into bulk waves and the results of our calculations could well be useful in the design of filters for SAW and more generally of periodic transducers on piezoelectric materials.

In different works, the study was restricted to SH waves propagating at the periodically corrugated surface of an isotropic[5–15] or anisotropic[16] substrate. In this article, we have extended the problem and investigated SAW of a general polarization associated with the surface of a piezoelectric substrate supporting a periodic array of wires, e.g., electrodes of various aspects ratios, instead of shallow grooves or thin metal strips as usually studied. As described in Sec. II, we have used an efficient computational tool based on the combination of finite element analysis and a boundary integral method.[17] This approach allows one to calculate the admittance of an interdigitated transducer (IDT), which is a basic tool for predicting the waves parameters, and has been extended in this work to obtain the polarization of the electro-acoustic waves. The main feature in this respect lies in the calculation of surface waves with a coupled polarization in anisotropic media, namely piezoelectric substrates. In addition, the IDT response predicted in this work is a good tool for a comparison with experiments that are feasible using SAW technology. In Sec. III, we discuss the frequency behavior of the localized modes as a function of the electrode height compared to the period ($h/2p$) for different materials, i.e., Y+128 lithium niobate, Y+36 lithium tantalate, and Y+42.75 quartz with either X propagation or Z propagation. These particular cuts are among the most widespread in SAW technology. We also identify the polarization of these localized modes. As will be seen, we find modes of a transverse type, as can be expected, but also modes mostly polar-

a)Electronic mail: vincent.laude@lpmo.edu

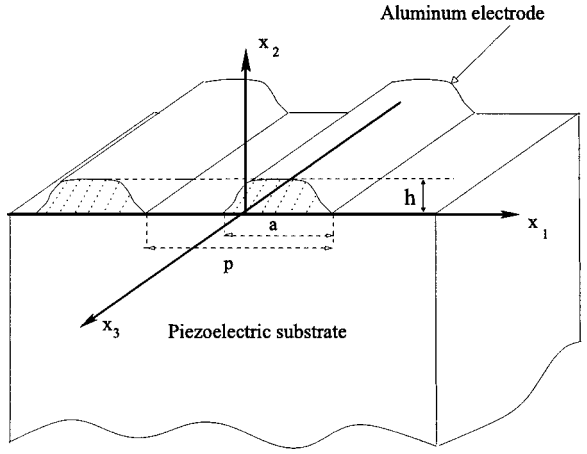

FIG. 1. Schematic of the geometry investigated in this work is shown.

ized in the sagittal plane, and generally polarized modes. Conclusions are drawn in Sec. IV.

II. MODEL

The definitions of the axes and the considered geometry are given in Fig. 1. The structure is composed of a semi-infinite piezoelectric substrate extending in the half-space $x_2<0$, whose surface supports a periodic infinite metal strip grating. The grating electrodes are parallel to axis x_3, centered at $x_1=np$, where n is the electrode index and p is the grating period. The width of the electrodes is denoted by a, so that a/p is the so-called metalization ratio. The electrodes are assumed to be long enough along x_3 such that any dependence in x_3 can be omitted in the following equations. All considered fields are supposed to exhibit a time dependence $\exp(jwt)$, where j is the imaginary constant and ω is the angular frequency.

A harmonic excitation is assumed to be applied to the infinite periodic grating, yielding the following form for the driving potential applied to the grating electrodes[18–20]

$$V_n(\gamma)=V_0\exp(-j2\pi n\gamma), \tag{1}$$

where γ is the characteristic parameter of the harmonic excitation. The alternating potential $+V$ and $-V$ usually considered for a practical electrical excitation corresponds to $\gamma=1/2$. For such a harmonic excitation, it has been shown that the currents of the electrodes have the same dependence as their voltages[17] and that the ratio $I_n(\gamma)/V_n(\gamma)$ does not depend on the actual number n of the electrode. It is the so-called strip admittance which was first introduced by Blötekjaër *et al.*[18,19] and is also referred to as the harmonic admittance (HA).[20] It is simply defined as

$$Y(\gamma)=\frac{I_n(\gamma)}{V_n(\gamma)}. \tag{2}$$

The determination of the grating HA has been the main goal of many theoretical and numerical works; we use in this article, a method from Ventura *et al.*[17] The addressed problem is treated using an integral representation of the substrate surface assuming a semi-infinite medium, through a boundary integral method (BIM), connected through a discrete formulation to the diffracting elements in the structure, i.e., the electrodes, by finite element analysis (FEA). The BIM is based on the Green's function that relates the surface displacements to the surface stresses via a convolution operation. Note that the method of Ventura *et al.*[17] was originally termed for finite element method/boundary element method, but we prefer the more accurate FEA/BIM terminology. Considering the harmonic excitation of Eq. (1), only one period of the infinite grating has to be considered in the analysis and the convolution relation can be written

$$u_i(x_1)=\int_{-\frac{p}{2}}^{+\frac{p}{2}} G_{ij}^{(p)}(x_1-x')t_{j2}(x')dx', \tag{3}$$

where $G_{ij}^{(p)}$ is the periodic Green's function defined as

$$G_{ij}^{(p)}(x_1)=\sum_{q=-\infty}^{+\infty}\hat{G}_{ij}(\gamma+q)\exp(j2\pi(q+\gamma)x_1/p). \tag{4}$$

In Eq. (3), u_i and t_{j2} are, respectively, the components of the generalized surface displacement and stress, and u_4 and t_{42} are, respectively, the surface electrical potential ϕ and the surface charge density Q, i.e., the difference between the normal component of the electrical displacement in air and in the substrate. $\hat{G}_{ij}$ is the Fourier transform of the surface Green's function, i.e., the spectral Green's function. Its expression for an arbitrary piezoelectric material can be found for instance in Ref. 20.

As proposed by several authors,[21,22] a Chebyshev polynomial expansion of the electromechanical fields is inserted in Eq. (3) as

$$\begin{cases} t_{2j}(x_1)=\dfrac{1}{\sqrt{1-\overline{x}^2}}\displaystyle\sum_{m=0}^{+\infty}C_{t_{2j}}^{(m)}T_m(\overline{x}) \\ Q(x_1)=\dfrac{1}{\sqrt{1-\overline{x}^2}}\displaystyle\sum_{m=0}^{+\infty}C_{Q}^{(m)}T_m(\overline{x}) \end{cases}, \tag{5}$$

$$\begin{cases} u_i(x_1)=\displaystyle\sum_{m=0}^{+\infty}C_{u_i}^{(m)}T_m(\overline{x}) \\ \phi(x_1)=\displaystyle\sum_{m=0}^{+\infty}C_{\phi}^{(m)}T_m(\overline{x}) \end{cases}, \tag{6}$$

where the expansion is only applied at the interface Γ between the substrate and the electrode ($|x_1|<a/2$) and $\overline{x}=2x_1/a$. In Eqs. (5) and (6), the electrode is assumed to be symmetric and centered at the origin, extending along x_1 from $-a/2$ to $a/2$, and T_m represents the Chebychev polynomial of order m. $\{C_f^{(m)}\}$ is the vector of the Chebyshev expansion coefficients for the considered function f. In addition to Eq. (5), it is assumed that the stress t_2 and electrical charge Q are zero in between the electrodes. By inserting Eqs. (4) and (6) into Eq. (3), the following equation relating the Chebyshev expansion coefficients can be obtained for the electromechanical behavior of the substrate[17]

$$\begin{Bmatrix} C_{u_i}^{(m)} \\ C_{\phi}^{(m)} \end{Bmatrix}=\begin{bmatrix} A_{ut} & A_{uQ} \\ A_{\phi t} & A_{\phi Q} \end{bmatrix}\begin{Bmatrix} C_{t_{2j}}^{(n)} \\ C_{Q}^{(n)} \end{Bmatrix}. \tag{7}$$

It is generally accepted that an infinitely thin electrode can be assumed for the electrical behavior of the metal. This is because the dielectric permittivity is much larger in the substrate than it is in air or in a vacuum, causing charges to be mostly localized at the interface between the electrodes and the substrate. This assumption will be made here. However, it has been shown that the mechanical (acoustic) contribution of the strip must be taken into account[9] and is here modeled using FEA. The result of this analysis, projected onto the Chebyshev polynomial expansion, can be symbolically written as[17]

$$\{C_{u_i}^{(m)}\}=\frac{1}{p}\left[\int P_k T_m\right][K-\omega^2 M]_{\Gamma,kl}^{-1}\left[\int P_l T_n\right]\{C_{t_{2j}}^{(n)}\}, \tag{8}$$

where $[K-\omega^2 M]_\Gamma$ is the usual finite element factorization matrix, where the subscript Γ indicates that it is restricted to the electrode–substrate boundary. Matrix notation $[\int P_k T_m]$ represents the conversion of the Chebychev's expansion to a FEA polynomial interpolation P. In this study, we use second degree Lagrange polynomials for FEA, but first degree polynomials can also be used without any loss of precision using moderately dense meshes (200 to 300 nodes). The mechanical contribution of the electrode can then be expressed in matrix form as

$$\{C_{u_i}^{(m)}\}=B_{ut}\{C_{t_{2j}}^{(n)}\}. \tag{9}$$

The electrical boundary condition under the electrode at the origin is that the potential ϕ is constant and equal to V_0. From this condition the vector $C_\phi^{(m)}$ is easily determined. The mechanical contribution in Eq. (7) can be eliminated by inserting Eq. (9), and the resulting system solved for $C_Q^{(n)}$. The total electrical charge Q_0 under the electrode is computed by integration of the charge density. The result is[17]

$$Y(\gamma)=j\frac{\pi}{2}\omega a\left(\frac{C_Q^{(0)}}{V_0}\right). \tag{10}$$

Though much work has been devoted to the computation of the HA including mass loading effects, the mechanical displacement under the electrodes is rarely computed and almost never exploited. However, this information is required to estimate the wave polarization. To this aim, the calculation of the expansion coefficients of mechanical displacements can be obtained by inserting Eq. (9) into Eq. (7), which gives access to a relation between the mechanical displacements and the electrical charge expansion coefficients

$$\{C_{u_i}^{(m)}\}=B_{ut}\{C_{t_{2j}}^{(n)}\}=-B_{ut}[A_{ut}-B_{ut}]^{-1}A_{uQ}\{C_Q^{(n)}\}, \tag{11}$$

where the vector $\{C_Q^{(n)}\}$ has already been computed for the calculation of the HA. We propose to estimate the polarization of the elastic wave as the mean quadratic value of the mechanical displacements under the electrodes, through the definition

$$\langle u_i\rangle^2=\frac{\int_{-\frac{a}{2}}^{+\frac{a}{2}}|u_i^2(x_1)|dx_1}{\int_{-\frac{a}{2}}^{+\frac{a}{2}}dx_1}=\int_{-1}^{+1}|u_i^2(\bar{x})|d\bar{x}. \tag{12}$$

Using Eq. (6) and performing the resulting integrals, the following relation is obtained

$$\langle u_i\rangle^2=\sum_{m=0}^{+\infty}\sum_{n=0}^{+\infty}C_{u_i}^{(m)*}C_{u_i}^{(n)}R_{mn}, \tag{13}$$

where the scalar products of the Chebychev polynomials are gathered in matrix R_{mn} whose expression is

$$R_{mn}=\frac{1}{2}\left(\frac{1}{m+n+1}+\frac{1-\delta(m-n+1)}{m-n+1}-\frac{1-\delta(m+n-1)}{m+n-1}-\frac{1-\delta(m-n-1)}{m-n-1}\right). \tag{14}$$

We insist that the definition of Eq. (12) has some degree of arbitrariness. One could have chosen another definition instead, such as the mean value of the displacements in the whole period. However, both measures should give similar values.

III. RESULTS AND DISCUSSION

In this section, we discuss the existence of modes of general polarization propagating as (quasi) surface waves along the interface between a piezoelectric substrate and a metallic grating with arbitrary electrode height. In the examples discussed next, the piezoelectric substrate is either Y+128 lithium niobate ($LiNbO_3$), Y+36 lithium tantalate ($LiTaO_3$), or Y+42.75 quartz (SiO_2) with either X or Z propagation. The metal is taken to be aluminum, since it is widely used for SAW devices. The electrode shape is taken to be rectangular in all numerical simulations.

In the search for modes, we use the theoretical developments of the preceding section, and more particularly the HA and the displacements given by Eqs. (10) and (13), respectively, with an electrical excitation of the structure described by $\gamma=1/2$, i.e., with an alternating potential $\pm V_0$. Following this approach, only piezoelectrically coupled modes can be identified. One should note that in the most general case, e.g., for triclinic materials or rotated crystal cut without any particular symmetry, the wave excitation caused by piezoelectricity gives rise to an elastic polarization in which the three components of the mechanical displacement contribute.

In the structure depicted in Fig. 1, there are three independent parameters, i.e., the frequency f, the period p, and the electrode height h. However, using the period as a dimensioning parameter, it is sufficient to use the reduced parameters fp and $h/2p$. At resonance, the wavelength is imposed by the grating to be exactly $2p$. Then $fp=v/2$ is half the phase velocity at resonance, and $h/2p$ is the ratio of the electrode height to the wavelength at resonance.

Figure 2 shows the admittance and the average polarization as defined by Eqs. (10) and (13), respectively, as a function of fp for $h/2p=1$, for a Y+128 lithium niobate sub-

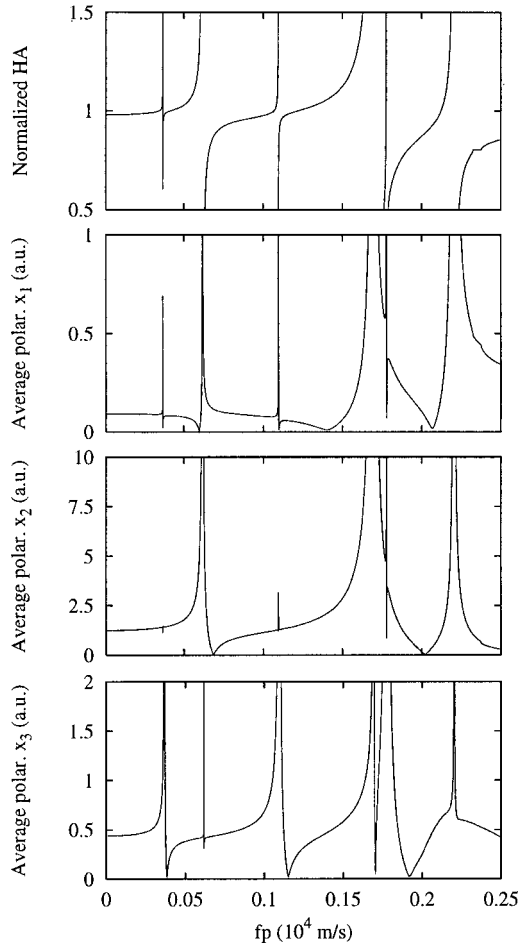

FIG. 2. Frequency dependent response of the corrugated surface of a Y+128 lithium niobate substrate, (a) normalized harmonic admittance, (b) average polarization along axis x_1, (c) average polarization along axis x_2, and (d) average polarization along axis x_3 are shown.

strate. Exactly six poles can be observed, each corresponding to a valid piezoelastic mode of the corrugated surface. The frequency-period products for which these modes appear are listed in Table I. For each of these modes, there exists a frequency stop band, and it is easy to find the synchronism frequency (or resonance frequency) from the position of the pole, i.e., the position of the maximum in admittance. It is observed also that these maxima are coincident with the polarization maxima. It can be seen that the modes are not purely polarized along one of the axes x_1, x_2, and x_3, but that they are each preferentially polarized either in the sagittal (vertical) plane (x_1, and x_2) or along axis x_3. In the following, we refer to VP or SH modes as vertically polarized modes or shear horizontal modes, respectively. The polarization of VP modes is then a combination of shear vertical (SV) and longitudinal displacements. In Fig. 2, it can be seen that the first, third, and fifth modes are SH modes, while the second, fourth, and sixth modes are VP modes. As was stated in the introduction, for an isotropic substrate, only purely transverse or SH modes have been discussed. For a piezoelectric substrate such as Y+128 niobate, VP modes are found as well.

TABLE I. Frequency-period product at resonance and polarization type for each of the six piezo-elastic modes of Fig. 2 (Y+128 lithium niobate substrate and $h/2p=1$) are presented.

Mode number	1	2	3	4	5	6
fp (m/s)	368	618	1096	1693	1778	2204
type	SH	VP	SH	VP	SH	VP

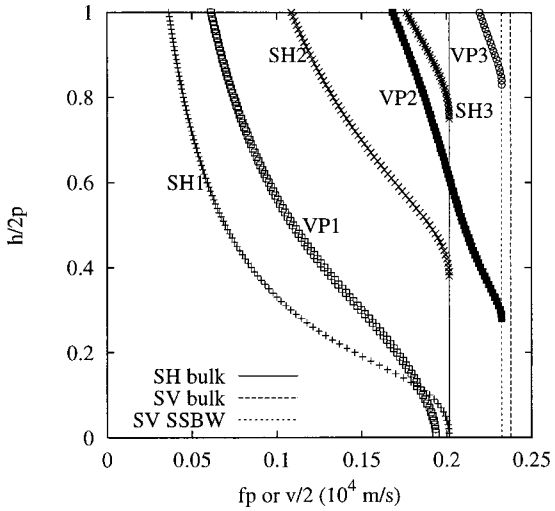

FIG. 3. Dispersion of the modes of the corrugated surface as a function of the electrode height for a Y+128 lithium niobate substrate is shown.

The numerical results of Fig. 2 give relevant information about the existence and the polarization of the modes of the corrugated surface. It is then natural to wonder about the evolution of these modes as a function of the electrode height. For each mode, we then start from a rather large value of $h/2p$, e.g., $h/2p=1$, and gradually decrease this parameter while following the synchronism frequency and the polarization of the mode, through a simple search for the maxima. In this way, we obtain the dispersion curves of Fig. 3 in the case of a Y+128 lithium niobate substrate. The same computations repeated for Y+36 lithium tantalate and Y+42.75 quartz with either X propagation or Z propagation lead to Figs. 4, 5, and 6, respectively. Many observations can be made regarding these dispersion curves. We will discuss extensively the dispersion curves for Y+128 lithium niobate in Fig. 3, and then outline the differences observed with the other substrates.

The mode velocity is always found to decrease as the thickness increases, in accordance with the usual mass loading effect associated with the electrodes. For instance, the VP1 mode velocity is reduced for $h/2p=0.5\%$ to 56% of its value for an infinitely thin electrode, and to 32% for $h/2p=1$. It is clearly seen that the velocity of SH modes is more affected by the electrode thickness than is the velocity of VP modes. As a consequence, the dispersion curves for SH and VP modes can cross, as is for instance seen for the SH1 and VP1 modes.

The dispersion curves are well defined and smooth, and have a lower cut-off frequency. Except for the VP1 mode, this cut-off frequency is clearly associated with a bulk wave in the substrate of a polarization similar to that of the surface mode, i.e., a SH mode originates for some thickness from a

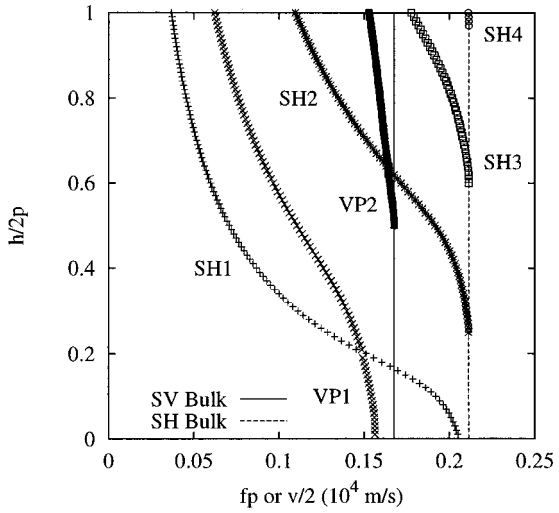

FIG. 4. Dispersion of the modes of the corrugated surface as a function of the electrode height for a Y+36 lithium tantalate substrate is shown.

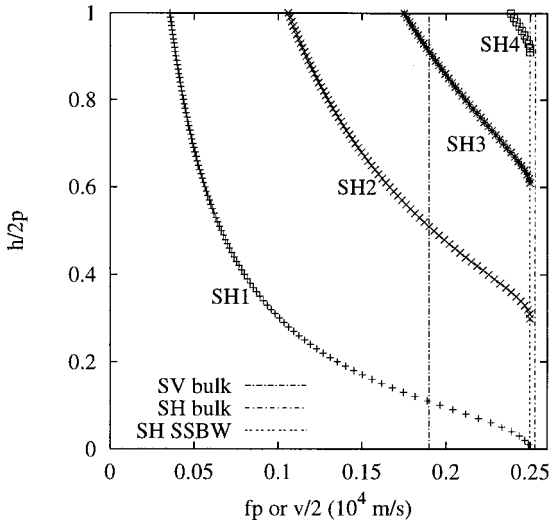

FIG. 6. Dispersion of the modes of the corrugated surface as a function of the electrode height for a (Y+42.75 and Z) quartz substrate is shown.

SH bulk wave, and a VP mode originates for some thickness from a SV bulk wave, since the latter is slower than the longitudinal bulk wave. Because they are independent of the electrode height, the bulk wave velocities in the substrate appear as vertical lines, and define band limits. In the case of VP1, the cut-off frequency is connected to the Rayleigh wave velocity in the substrate. The VP1 mode is the usual Rayleigh SAW that exists even on the noncorrugated surface. It is in this case the only surface mode that exists for zero thickness of the electrodes. In the case of VP modes, the VP bulk wave velocity is not the bulk wave velocity for a zero phase angle (with a wave vector along x_1) as is the case for the SH bulk wave velocity, but the velocity of a surface skimming bulk wave (SSBW) having a zero group angle and a nonzero phase angle. The SH bulk wave is also a SSBW, i.e., it has both zero group angle and phase angle. It is interesting to note that the VP2 and VP3 modes are similar to leaky SAW for lower thicknesses until their dispersion curves reach the SH bulk wave velocity, and that after that point they become similar to true SAW. Since always slower than any radiated bulk wave, the VP1 mode is always a true SAW.

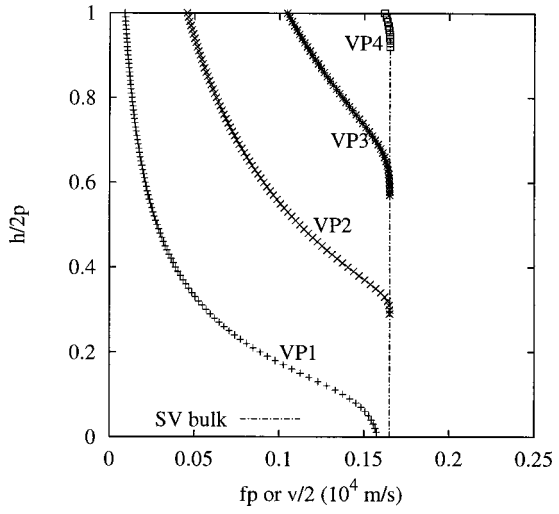

FIG. 5. Dispersion of the modes of the corrugated surface as a function of the electrode height for a (Y+42.75 and X) quartz substrate is shown.

The dispersion curves for Y+36 lithium tantalate depicted in Fig. 4 are similar to that of Y+128 lithium niobate but for the following differences. First, two surface modes exist for zero thickness, SH1 and VP1, and are respectively the Rayleigh SAW and the well-known leaky SAW of Y+36 tantalate. Second, both SH and VP bulk waves are SSBW's. As in the case of Y+128 lithium niobate, the velocity of SH modes is more affected by the electrode thickness than is the velocity of VP modes, which again results in the crossing of the dispersion curves for SH and VP modes, as is for instance seen for the SH1 and VP1, and SH2 and VP2 modes, respectively.

The dispersion curves for Y+42.75 quartz with X propagation are depicted in Fig. 5, and are rather different from the dispersion curves for Y+128 lithium niobate and Y+36 lithium tantalate, in the sense that no SH mostly modes are found, but only VP mostly modes. It should be noted however that the VP mostly modes include some polarization along axis x_3, so that their actual polarization is general.

The dispersion curves for Y+42.75 quartz with Z propagation are depicted in Fig. 6. In this case, only SH modes are observed. It is known[9,14,22] that for this cut and this propagation direction only pure shear waves can be excited by the piezoelectric effect. Indeed, an inspection of the average polarization computed using Eq. (12) reveals that it is strictly zero in the sagittal plane. This cut is the only one considered in this work for which we have found purely polarized modes.

IV. CONCLUSION

In this work, we have analyzed the behavior of SAW with general polarization propagating under a periodic array of metallic electrodes with a large aspect ratio, deposited over a piezoelectric substrate. To achieve this goal, we have modified an efficient computational tool based on the com-

bination of FEA and a BIM. This method allows one to calculate the admittance of an IDT, which is a basic tool for predicting the waves parameters, and has been extended in this work to obtain the polarization of the electro-acoustic waves. We emphasize that no assumptions have been made regarding the polarization structure of the solutions, and that the electrical and acoustic boundary conditions are properly taken into account.

It had been observed previously that SH SAW exist when the surface of an isotropic substrate is perturbed by a strong corrugation. In the case of piezoelectric substrates, widely used for SAW generation, no general analysis has been given before to the best of our knowledge. We have considered in our simulations a number of standard cuts of piezoelectric substrates, including Y+128 lithium niobate, Y+36 lithium tantalate, and Y+42.75 quartz with either X or Z propagation. The number and dispersion of the surface waves are very dependent upon the height of the aluminum electrodes, while their polarization is very dependent on the substrate. As the electrode height is gradually increased, SH surface waves start to appear in a fashion very similar to the isotropic substrate case. However, at the same time, we observe the appearance of VP surface waves that are mostly polarized in the sagittal plane. Both SH and VP surface waves undergo a deceleration of the phase velocity as the electrode height increases. These general trends indicate that a strong interaction occurs between the vibrations of high aspect ratio electrodes and surface waves of arbitrary polarization that are piezoelectrically excited. In some sense, the observed SH surface modes are similar to Love modes of a layer deposited on a substrate, if the considered system of periodic electrodes separated by a vacuum is considered in a limiting sense as an effective homogeneous medium, with a mass density and elastic constants lower than that of bulk aluminum.[5]

ACKNOWLEDGMENTS

This work has been made possible partly thanks to the Convention 991/4269 First-Europe (''Objectif 1'') from the Walloonia Region of Belgium and the European Union. The authors acknowledge fruitful discussions with B. Djafari-Rouhani of Lille University, France.

[1] A. A. Maradudin, T. Michel, B. Djafari-Rouhani, A. R. Mc Gurn, and A. R. Baghai-Wadji. in *Continuum Models and Discrete Systems*, edited by G.A. Maugin (Longman, London, 1990), Vol. I.
[2] V. P. Plessky and A. W. Simonian, Phys. Lett. A **155**, 281 (1991).
[3] B. Djafari-Rouhani, L. Dobrzynski, and A. Khelif, J. Phys.: Condens. Matter **5**, 8177 (1993).
[4] B. Djafari-Rouhani L. Dobrzynski, and A. Khelif, Prog. Surf. Sci. **48**, 301 (1995).
[5] A. A. Maradudin, *Recent Developments in Surface Acoustic Waves*, edited by G. A. Maugin (Springer, Berlin, 1991).
[6] B. A. Auld, J. J. Gagnepain, and M. Tan, Electron. Lett. **12**, 650 (1976).
[7] Y. V. Gulyaev and V. P. Plessky, Zh. Tekh. Fiz. **48**, 447 (1978); Sov. Phys. Tech. Phys. **23**, 266 (1978).
[8] N. E. Glass and A. A. Maradudin, Electron. Lett. **17**, 773 (1981).
[9] A. R. Baghai-Wadji and A. A. Maradudin, Appl. Phys. Lett. **59**, 1841 (1991).
[10] A. P. Mayer, W. Zierau, and A. A. Maradudin, J. Appl. Phys. **69**, 1942 (1991).
[11] A. R. Baghai-Wadji, V. P. Plessky, and A. V. Simonian, Sov. Phys. Acoust. **38**, 442 (1992).
[12] B. Djafari-Rouhani and A. A. Maradudin, J. Appl. Phys. **65**, 4245 (1989).
[13] A. A. Maradudin and W. Zierau, Geophys. J. Int. **118**, 352 (1994).
[14] V. P. Plessky and T. Thorvaldsson, IEEE Trans. Ultrason. Ferroelectr. Freq. Control **42**, 280 (1995).
[15] B. Djafari-Rouhani and A. Khelif, Vacuum **54**, 309 (1999).
[16] A. N. Darinskii, J. Acoust. Soc. Am. **107**, 2447 (2000).
[17] P. Ventura, J. M. Hodé, and M. Solal, Proc. IEEE **95CH35844**, 263 (1995).
[18] K. Blotekjaer, K. A. Ingebrigtsen, and H. Skeie, IEEE Trans. Electron Devices **20**, 1133 (1973).
[19] K. Blotekjaer, K. A. Ingebrigtsen, and H. Skeie, IEEE Trans. Electron Devices **20**, 1139 (1973).
[20] Y. Zhang, J. Desbois, and L. Boyer, IEEE Trans. Ultrason. Ferroelectr. Freq. Control **40**, 183 (1993).
[21] M. Solal, P. Ventura, and J. M. Hodé, Proc. IEEE **94CH3468-6**, 263 (1994).
[22] V. P. Plessky and T. Thorvaldsson, Electron. Lett. **14**, 1317 (1992).